Chapter 1

Introduction

1.1 Unsteady Aerodynamics

The study of truly unsteady, high-excursion and high-Reynolds Number separated flows over submarines, aircraft or missiles has become of great importance in the analysis and the improvement of the dynamic performance. Because of highly complex, three-dimensional, turbulent and separated nature, standard stability derivative techniques fail to capture the nonlinearities in these flows and Computational Fluid Dynamics (CFD) techniques need physical models that can resolve the complexities of such flow fields in order to get accurate and more reliable results. Suitable simulation of the time-dependent maneuvers in the wind tunnels is not only important for understanding the physics of complex flow phenomena, but also supplies the necessary information required for developing the realistic unsteady physical flow models. The DyPPiR (Dynamic plunge-pitch-roll) model mount, a computer controlled, three degrees of freedom robotic arm at the Stability Wind Tunnel of Virginia Tech, provides the unique capability of performing pre-programmed general, high-excursion, large scale, high-Reynolds Number unsteady maneuvers [4].

Dynamic testing has been an important part of design and validation of various types of craft for decades. Typically these techniques are only *quasi-steady*, relying on very small amplitude sinusoidal oscillations that can describe small-excursion maneuvers reasonably well [2]. As discussed by Wetzel and Simpson [3], there is a significant difference between

quasi-steady and unsteady aerodynamics. In a quasi-steady approach, the aerodynamics of a maneuvering body are dependent only on the instantaneous state of the model (α angle of attack, β sideslip angle, control surface deflections, etc.), whereas in fully general unsteady aerodynamics, explicit time dependency, or history effects are also included. Mathematically the distinction between quasi-steady and unsteady aerodynamics can be shown as follows: steady, $\mathbf{F}(\alpha, \beta, ...)$; quasi-steady, $\mathbf{F}[\alpha(\mathbf{t}'), \beta(\mathbf{t}'), ...]$; and fully unsteady $\mathbf{G}[\mathbf{t}', \alpha(\mathbf{t}'), \dot{\alpha}(\mathbf{t}'), \beta(\mathbf{t}'), \dot{\beta}(\mathbf{t}'), ...]$ where $\mathbf{F}$ and $\mathbf{G}$ can be a dominant flow feature such as separation location. Here t' is the non-dimensional time defined by Etkin [5]:

$$t' = \frac{t}{t_{ref}} = \frac{tU_\infty}{L} \tag{1.1}$$

t_{ref} represents the time for the flow to pass over a model: L/U_∞. The non-dimensional time t' relates the unsteady wind tunnel tests to the real-time maneuvers. This non-dimensionalization follows the approach that is used to non-dimensionalize the variables in the equations of motion of aircraft dynamics [5] and it does not include any viscous terms. However the onset and the propagation of the three-dimensional unsteady flow separation, which is a frequent flow phenomena seen over a vehicle undergoing a typical, high-excursion, and truly unsteady maneuver, are strongly influenced by the viscous effects. Reynolds number based on the model length (or any other appropriate characteristic length) $Re_L = \rho U_\infty L/\mu$ representing the ratio of the inertial forces to the viscous forces, is another important parameter to be considered during the unsteady wind tunnel testing. The type of the flow separation (laminar or turbulent), and the transition location on the model surface are strong functions of the Reynolds number until a *critical* value is reached. Beyond this critical value of Re_L, the separation type and locations become less sensitive to the Reynolds number effects. In some experiments, it may be impossible to simulate the real flow Reynolds number (such as Re_L for submarines, big transport airplanes etc.) due the model size or the wind tunnel speed limitations. In this study and some of the previous unsteady experiments done at Virginia Tech, specially designed boundary layer trips are used to simulate higher Reynolds number flows and to fix the transition location that will produce a less Reynolds-number-sensitive separation.

Besides quantitative differences between the steady and the unsteady aerodynamic parameters such as the skin-friction, force and moment coefficients, the qualitative nature of the unsteady flow fields also differ from the steady ones. In fact, the quantitative variations are the results that originate from flow topology differences between the steady and

the unsteady flow fields. As an example, in the crossflow separation phenomena discussed in this study and previous prolate spheroid work [2], the history effects mainly cause time lags between the unsteady and the corresponding quasi-steady flow fields, which can be quantified by measuring the flow separation locations. Approximating these time lags by the models that can explain the *real physics* of the three-dimensional, turbulent, unsteady flow separation is a big challenge in the field of aerodynamics as well as acquiring unsteady data. One of the main purposes of this study is to apply such an approximation to the unsteady separation locations measured on the DARPA2 model.

1.2 Three-Dimensional Separations

Both the steady and the unsteady flow fields over the DARPA2 model used in this study are dominated by the three-dimensional flow separation after a certain angle of attack. As described by Simpson [6], separation is the entire process of *departure* or *breakaway*, or the breakdown of the boundary layer flow. An abrupt thickening of the rotational-flow region next to a wall and significant values of the normal-to-wall velocity component V must accompany breakaway, or otherwise this region will not have significant interaction with the inviscid free-stream flow. As can be seen from figure 1.1, surface skin-friction lines converge on each side of the separation line. Along this separation line, there exists a stream surface across which no flow from one side of the separation line can pass to the other side.

Three-dimensional (3-D) separations can be classified in three groups with respect to their topology and kinematics (figure 1.1): (a) horseshoe type; (b) Werle type; and (c) crossflow separations. In Yates and Chapman [1], horseshoe and Werle type separations are defined as *global separations* (or *closed separations*). These always have a saddle point of separation on the surface. Figure 1.1 (c) shows the local or the crossflow separation topology. No 3-D critical points on the surface or in the flow can be observed in such type of flows and the center of a separated vortex structure has minimum streamline curvature.

The horseshoe type and the crossflow separation are of particular interest in this study: the flow field in the vicinity and the downstream of the sail is dominated by the horseshoe type separation and the crossflow separation is the main flow characteristic on the leeside

of the DARPA2 model at an angle of attack for steady and the unsteady measurements. The circumferential pressure gradient is the dominant factor in the crossflow separation process. Figure 1.2 shows the on-axis cross sectional view of the secondary flow streamlines from a crossflow separation: S1 is the primary separation location and S2 stands for the secondary separation location. R1 and R2 locate the primary and the secondary reattachment positions. At low angles of attack, only the primary separation is observed on the leeward side of the model and as the angle of attack increases the primary separation line moves towards the windward side. After a certain angle of attack, the secondary separation line on the leeward side of the model can be observed.

Besides qualitative verification of the crossflow separation, one is also interested in finding the actual values of the separation locations. Simpson [6] shows that the wall shear provides lower order information about the separation location than the pressure by analyzing the continuity and the momentum equations near the wall:

$$V = -\frac{1}{2\mu}\left(\nabla \cdot \vec{\tau_w}\right) y^2 + \frac{1}{6\mu}\left(\nabla^2 p\right) y^3 + \ldots \tag{1.2}$$

Time-averaged wall pressure measurements are relatively insensitive to the flow separation and only *massive* separations are detected from time-averaged wall pressure measurements [6]. In order to use equation 1.2 rigorously, the entire wall shear direction and the magnitude fields should be known to perform the divergence operation on the right hand side for finding normal-to-wall velocity V at all points on the body and to determine the separation location. This approach is impractical due to the large number of sensors that should be used. As an alternative, Simpson et al. [7] showed that the local minimum of the circumferential skin-friction distribution is a good approximation of separation location. By using this fact, directionally insensitive hot-film sensors are used to measure the magnitudes of the skin-friction on the model surface in this study. The local minima are used for the determination of the steady and the unsteady separation locations.

1.3 Previous Studies

Table 1.1 gives a summary of the test conditions from some previous unsteady three-dimensional aero/hydrodynamic experiments relevant to this study. In the last row of

Table 1.1: Summary of the test conditions from some unsteady aero/hyrodynamic experiments (modified from Wetzel and Simpson [3])

Authors	*Model*	*Tunnel*	Re_L	$\bar{\dot{\alpha}} = \dot{\alpha}\frac{L}{U_\infty}$	α *range*	*Measurements*
Gad-el-hak and Ho [8]	ogive cylinder	water	40,000	1.05	0 ° to 30 °	flow vis.
Montividas et al. [9]	cone cylinder	wind	56,650	0.7	0 ° to 90 °	flow vis., wake LDV
Smith and Nunn [10]	ogive cylinder	wind	1,200,000	0.0405	−15 ° to 105 °	flow vis., force & moments
Panzer et al. [11]	hemisphere cylinder	wind	229,000	0.0065	15 ° to 30 °	wake LDV
Panzer et al. [11]	hemisphere cylinder	water	75,000	0.1	15 ° to 30 °	wake LDV
Brandon and Shah [12]	F-18	wind	1,600,000	0.0364	−10 ° to 80 °	flow vis., force, & moments
Wetzel and Simpson [3]	6:1 prolate spheroid	wind	4,200,000	0.047	0 ° to 30 °	hot-film
Whitfield [13]	DARPA2 Suboff	wind	5,500,000	0.076	0 ° to 25 °	force & moments
Hosder (current study)	**DARPA2 Suboff**	**wind**	**5,500,000**	**0.071**	1 ° **to** 27 °	**hot-film**

this table, information about the current work is presented. The maneuvers performed for all the experiments shown are the pitchup motions. The model geometry, experimental facility, Reynolds number Re_L, non-dimensional pitch rate $\bar{\dot{\alpha}}$, α range, and the measurement technique of each study can be compared by using table 1.1. In terms of Re_L, the prolate spheroid study of Wetzel and Simpson [3], DARPA2 Suboff study of Whitfield [13] and the present study can be considered as the only experiments that have high Reynolds number well above the critical value. Therefore the separation locations in these experiments are least likely to be sensitive to the Reynolds number effect. These three studies are performed at Virginia Tech Stability Wind Tunnel with the DyPPiR

and the boundary layer tripping are used for all three. The current study uses the same model geometry and the maneuver type as the ones in Whitfield's force and moment study [13]. In fact these two experiments are complementary in the sense that different measurement techniques are used to describe the whole picture of the same unsteady phenomena over the same geometry.

Among the previous studies, the unsteady crossflow separation location measurements on a maneuvering 6:1 prolate spheroid model by Wetzel and Simpson [3] can be considered as the most similar work to the one presented here in terms of the experimental measurement technique and the unsteady high-excursion maneuvers performed. In that study, they have determined significant lags in the unsteady flow separation locations on the prolate spheroid undergoing pitch-up and turning maneuvers compared with the steady data. Wetzel and Simpson [3] also found that a first-order lag model fits the unsteady data. Present work and the prolate spheroid study are the only experiments that utilize fine spatial resolution surface hot-film measurements to determine the unsteady skin-friction magnitudes and the separation locations on a maneuvering body. Most of the previous work uses different techniques and focuses on flow features other than separation, such as vortex location and breakdown [3].

1.4 Present Work

In the present work, unsteady turbulent surface flow on a maneuvering DARPA2 submarine model is studied. Hot-film sensors are used to measure the steady and the unsteady skin-friction magnitudes over the body surface. Local minima of the skin-friction magnitude are used to determine the separation locations. Steady skin-friction measurements are obtained at fourteen steady angles of attack. Unsteady maneuvers include the ramp pitchup maneuvers simulated by the DyPPiR. Mean wall static pressures are measured at 10° and 20° angles of attack. Surface oil flow visualizations are also used in order to examine the steady surface flow topology and the separation locations qualitatively. Both steady and unsteady tests are performed for two model configurations: The barebody (axisymmetric case) and the body with the sail (sail-on-side case).

Steady and the unsteady results obtained in this study give valuable information about the complex surface flow structure over the DARPA2 submarine model. The steady skin-

friction values and mean pressure measurements are used to describe the steady flow-field topology. Unsteady data show the difference between the steady and the unsteady flow-fields, especially in the separation topology. In this study, a first-order time lag model is used to approximate the unsteady data. The results of this approximation as well as the unsteady data may supply important information to the development of the realistic flow models to be used in calculating the unsteady 3-D flows over complex geometries.

The organization of the chapters here can be summarized as follows. In chapter 2, the experimental apparatus, facilities and techniques are described. This chapter gives the details about the DyPPiR, hot-film sensors, constant temperature anemometers and the pressure measurement system used in the experiments. The wind tunnel model including the geometry, different configurations and integration of the sensors is also described. Chapter 3 gives the test conditions and describes the steady measurements and the unsteady maneuvers performed in this study. Calibration of the hot-film sensors is explained in chapter 4. Chapter 5 includes the results obtained from the steady skin-friction and pressure measurements. The discussion about the data and conclusions based on the steady results are presented. The steady data reduction procedure both for the hot-film and the pressure measurements is also described in this chapter. The unsteady results and the data reduction procedure are presented in chapter 6. The unsteady flow topology and the differences between the steady and the unsteady flow fields are discussed. This chapter also includes the algebraic and the first-order time lag model approximations to the unsteady separation location data. Discussion about the unsteady data and the time lag approximation results are given. The last chapter presents the overall conclusions obtained from this study. Uncertainties in the measured skin-friction values and the related uncertainity calculations are included in the appendices.

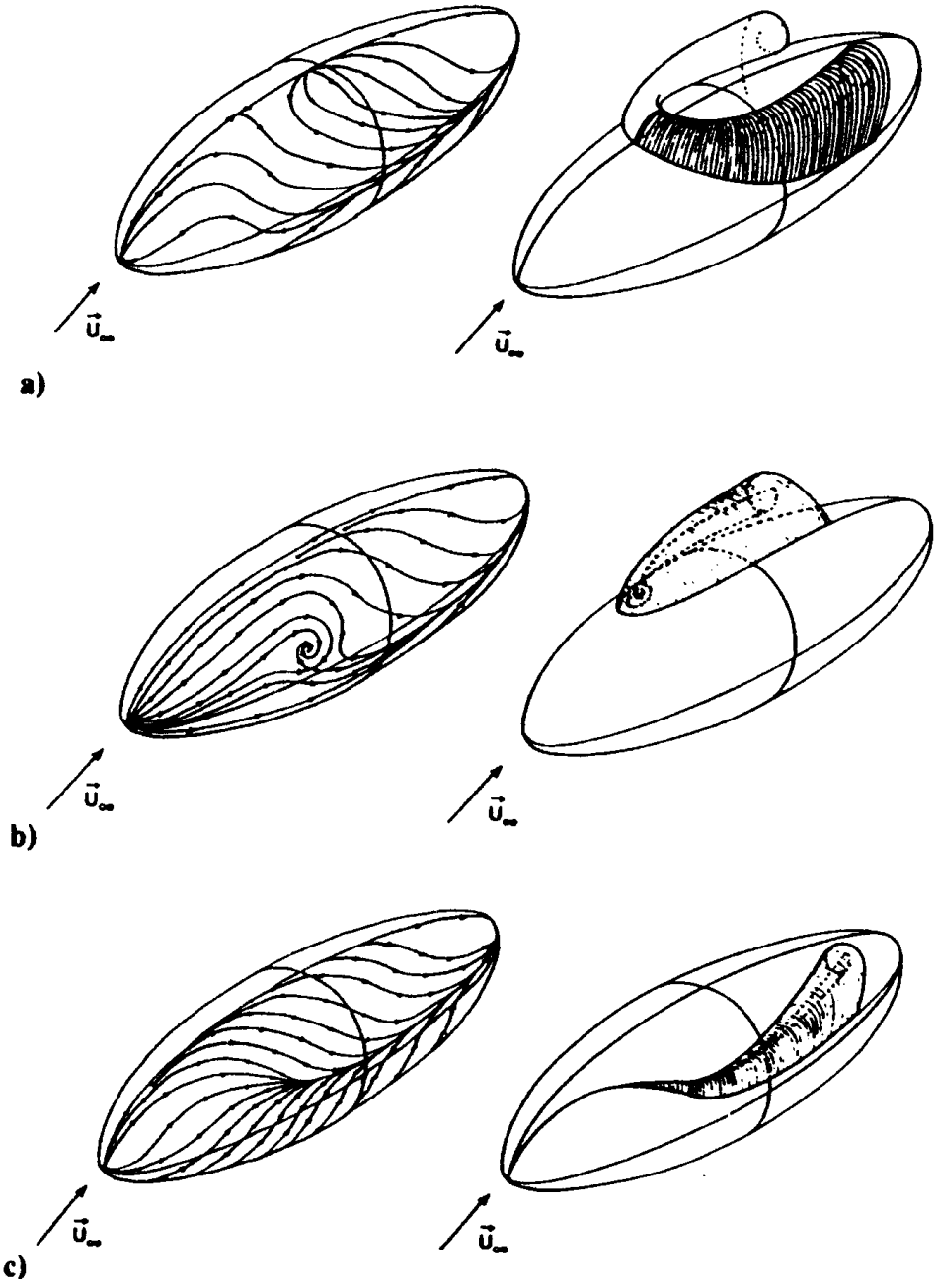

Figure 1.1: Limiting streamline pattern and surfaces of separation for three types of 3-D separation:(a) horseshoe type separation; (b) Werle type separation (the view of the surface separation is rotated $90\,^{\circ}$ from the view of the limiting streamline pattern); (c) cross flow separation. Taken from Yates and Chapman [1].

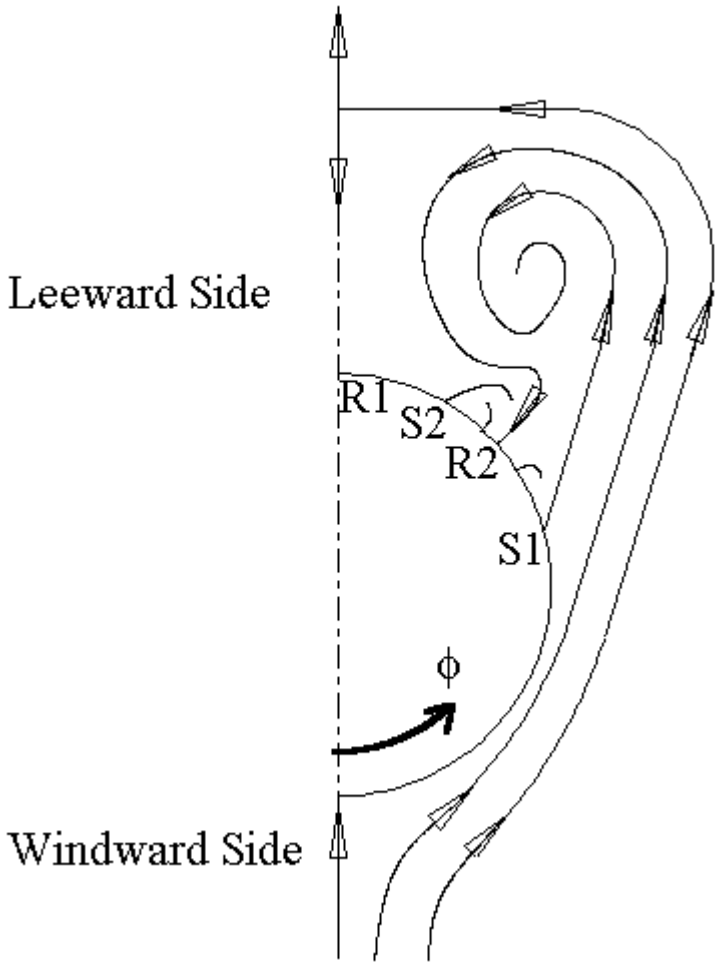

Figure 1.2: On-axis cross sectional view of secondary flow streamlines from a crossflow separation. P1: primary separation, P2: secondary separation, R1: Primary reattachment, R2: secondary reattachment.